Influence of a Nanoscale Gold Thin Layer on Ti/SnO_2-Sb_2O_5 Electrodes

Aicheng Chen* and Stephanie Nigro

Department of Chemistry, Lakehead University, Thunder Bay, Ontario P7B 5E1, Canada

Received: July 22, 2003; In Final Form: October 2, 2003

A nanoscale gold thin film and its influence on Ti/SnO_2-Sb_2O_5 coating have been investigated by scanning electron microscopy (SEM) and electrochemical methods such as cyclic voltammetry, electrochemical impedance spectroscopy (EIS), and the chronopotentiometric technique in both acidic and caustic solutions. The gold thin film was fabricated by sputtering, and its thickness was estimated using electrochemical methods. The nanoscale gold thin film on the titanium substrate exhibits electrochemical behavior similar to that of a polycrystalline Au electrode. Our study shows that the presence of a nanoscale Au thin film on the Ti substrate can effectively prevent the growth of a TiO_2 insulating layer between the substrate and the SnO_2-Sb_2O_5 coating, resulting either from the thermal procedure during the fabrication of the oxide electrodes or from the electrochemical process during the lifetime tests, thus greatly prolonging the service lifetime of the SnO_2-Sb_2O_5 electrodes. The failure mechanisms of the SnO_2-Sb_2O_5 electrodes have also been studied using the EIS and SEM techniques.

1. Introduction

The discovery of dimensionally stable anodes (DSAs) is one of the greatest technological breakthroughs of electrochemistry over the last 50 years.[1−3] DSAs are widely used in electrochemical processes including electrowinning, cathodic protection,[4,5] and remediation technology for a cleaner environment,[6−9] as well as in the chlorralkali industry.[10−12] Typically, DSAs consist of an active mixed-metal oxide (MMO) coating thermally deposited on a substrate, usually a valve metal (Ti, Zr, Ta, or Nb). Titanium is widely used as a substrate because of its good corrosion resistance and reasonable cost. The coating enables electrical charge transport between the base metal and the electrode/electrolyte interface. The MMO coating is also chosen for its high chemical and electrochemical stability and its ability to catalyze the desired electrochemical reaction. Several aspects, for instance, the microstructure, morphology, and operating conditions, significantly affect the stability of DSAs.[13−16]

One of the most probable deactivation mechanisms of DSAs is coating consumption.[17,18] This could be due to chemical consumption (interactions with electrolyte components or impurities), electrochemical consumption (e.g., electrooxidation and dissolution of noble metal oxides), and/or erosion (normally, the coating is porous, the gas evolution at the surface is very fast, and this can induce the detachment of some coating particles). Another possible failure mechanism is the formation of an insulating titanium oxide layer either due to the oxidation of the Ti substrate[19] or resulting from the selective loss of catalysts and active sites of the coatings.[20] Although tin- and antimony-based oxide electrodes (Ti/SnO_2-Sb_2O_5) are promising anodes for the electrochemical treatment of wastewater and groundwater because of their high overpotential for oxygen evolution, their ability to generate hydroxyl radicals and the lower cost compared to that of precious metal oxides, the commercial application of Ti/SnO_2-Sb_2O_5 is hampered by its short lifetime. Recent studies have shown that the addition of iridium oxide (IrO_2) to the SnO_2-Sb_2O_5 coating greatly increases its service life.[11] The electrochemical behavior of the Ti/IrO_2/SnO_2-Sb_2O_5 electrode lies between the performances of the Ti/IrO_2 and the Ti/SnO_2-Sb_2O_5 electrodes due to the incorporation of IrO_2 into the SnO_2-Sb_2O_5 coating during its preparation.[13] However, the addition of IrO_2 lowers the efficiency of the SnO_2-Sb_2O_5 electrodes for wastewater treatment as iridium oxides show a low overpotential for oxygen evolution.[21]

Particles with a grain size or layer thickness on a scale of 1−100 nm are called nanostructured materials. This nanoparticle size range is of particular interest due to the discernible changes in the electronic and structural properties of nanoparticles.[22,23] Gold nanoparticles have been extensively studied because of their unusually high catalytic activity for electrooxidation of CO and hydrocarbons.[24−26] In addition, gold exhibits excellent corrosion resistance and electrical conductivity. In the present work, we applied a thin gold film as an interlayer between the Ti substrate and the SnO_2-Sb_2O_5 coating. The thickness of the gold film was in the range between 6.8 and 13.6 nm as estimated by electrochemical methods. The electrochemical behaviors of the SnO_2-Sb_2O_5 coatings with and without the gold film interlayer were characterized using electrochemical methods such as cyclic voltammetry (CV), the galvanostatic technique, accelerated tests, and electrochemical impedance spectroscopy (EIS). The microstructural changes occurring in the electrodes before and after their lifetime tests were analyzed by scanning electron microscopy (SEM). The objectives of this study were (1) to study the electrochemical behavior of the nanostructured gold film on the Ti surface, (2) to investigate the effects of electrolytes on the service life of the SnO_2-Sb_2O_5 coating, (3) to determine the failure mechanisms of Ti/SnO_2-Sb_2O_5 electrodes, and (4) to study the influence of the nanostructured gold interlayer on the electrochemical behavior of Ti/SnO_2-Sb_2O_5 electrodes.

2. Experimental Section

A three-electrode cell system was used in this study as described in ref 27. The working electrodes Ti/SnO_2-Sb_2O_5 and

* To whom correspondence should be addressed. E-mail: aicheng.chen@lakeheadu.ca.

10.1021/jp036138w CCC: $25.00
Published on Web 11/07/2003

Ti/Au/SnO_2-Sb_2O_5 were prepared by the thermal decomposition technique. A grade 1 titanium rod with a 12 mm diameter was used as the substrate; thus, the geometric electrode surface area was 1.13 cm^2. The Ti substrate was polished first using silicon carbide grit 600 powder and then diamond compound paste (particle size <2 μm). To remove any remaining particles and degrease, the substrates were immersed in an acetone ultrasonic bath for 15 min. The samples were then etched in 32% HCl at a temperature of 85 °C for 15 min to remove the oxide layers and to provide a good adhesive surface for the coatings. The etched substrates were completely rinsed using ultrapure water. The gold film was applied to the pretreated substrates using a sputter (Ernest Fullam Inc.) for 1 or 2 min, denoted as Ti/Au1 or Ti/Au2, respectively. The amount of deposited Au was determined by weighing the sample before and after the Au deposition using a balance with a 0.01 mg precision. The average gold film load was 0.13 mg/cm^2 for 1 min of sputtering and 0.26 mg/cm^2 for 2 min of sputtering. The precursor solution was made by dissolving 0.20 g of $SbCl_3$ and 10.0 g of $SnCl_4 \cdot 5H_2O$ in 2.0 mL of concentrated 37% HCl and 98.0 mL of ethanol. The pretreated Ti substrate with and without the gold film interlayer was first dipped in the mixture of the precursor solution. The solvent was evaporated at around 80 °C by an air stream and then calcinated at 450 °C for 10 min. This procedure was repeated 12 times. A final 1 h postbaking at 450 °C completed the procedure. The coating load was in the range of 18.0−18.5 g/m^2. The microstructures of the pretreated Ti substrate and the oxide coating were characterized by SEM and X-ray energy-dispersive (EDX) spectrometry (JEOL 5900LV). The counter electrode was a Pt coil. Before each experiment the counter electrode was cleaned by flame annealing and then quenched with Millipore water. The reference electrode was a saturated calomel electrode (SCE) connected to the investigated solution through a salt bridge.

The electrochemical experiments such as CV, differential capacity (DC), galvanostatic measurements, and EIS were performed using a VoltaLab 40 potentiostat PGZ301. Electrochemical software VoltaMaster 4 (Version 5.1) was used for data acquisition and data analysis. The amplitude of the modulation potential for both the DC and EIS measurements was 10 mV, the frequency for the DC experiment was 25 Hz, and the range of frequency used for the EIS study was from 25 kHz to 0.025 Hz. The lifetime of a given electrode was determined using an accelerated test at 20 mA·cm^{-2} in either 1 M H_2SO_4 or 1 M NaOH solution. The electrode was said to be inactive when the anode potential reached 10 V vs SCE. The acidic 1.0 M H_2SO_4 solution was made with 99.999% sulfuric acid (Aldrich). The 1.0 M NaOH caustic solution was made from reagent-grade sodium hydroxide (Anachemia). Water was purified with a tandem Milli-Q water purification system (17.6 MΩ cm). All solutions were deaerated with ultrapure argon before the measurements, and argon was passed over the top of the solution during the experiment. All measurements were conducted at room temperature (20 ± 2 °C).

3. Results and Discussion

3.1. Microstructures of the Substrates, Gold Thin Films, and Oxide Coatings. The surface morphologies of the Ti substrate, gold film, and oxide coatings were examined by SEM. Figure 1 shows the SEM images of the Ti substrate etched in 32% HCl at 85 °C for 15 min (a) and the etched Ti with a gold thin film Ti/Au (b). It is clearly seen that the surface of the etched Ti substrates with or without the gold thin film is very rough. Figure 1c shows a typical SEM image of the SnO_2-Sb_2O_5 coating freshly prepared before electrochemical tests. There is no notable morphology difference between the SnO_2-Sb_2O_5 coating with or without the gold film interlayer. The SEM image shows that the SnO_2-Sb_2O_5 coating is compact; this observation is consistent with the previous studies performed by Comninellis et al.[13]

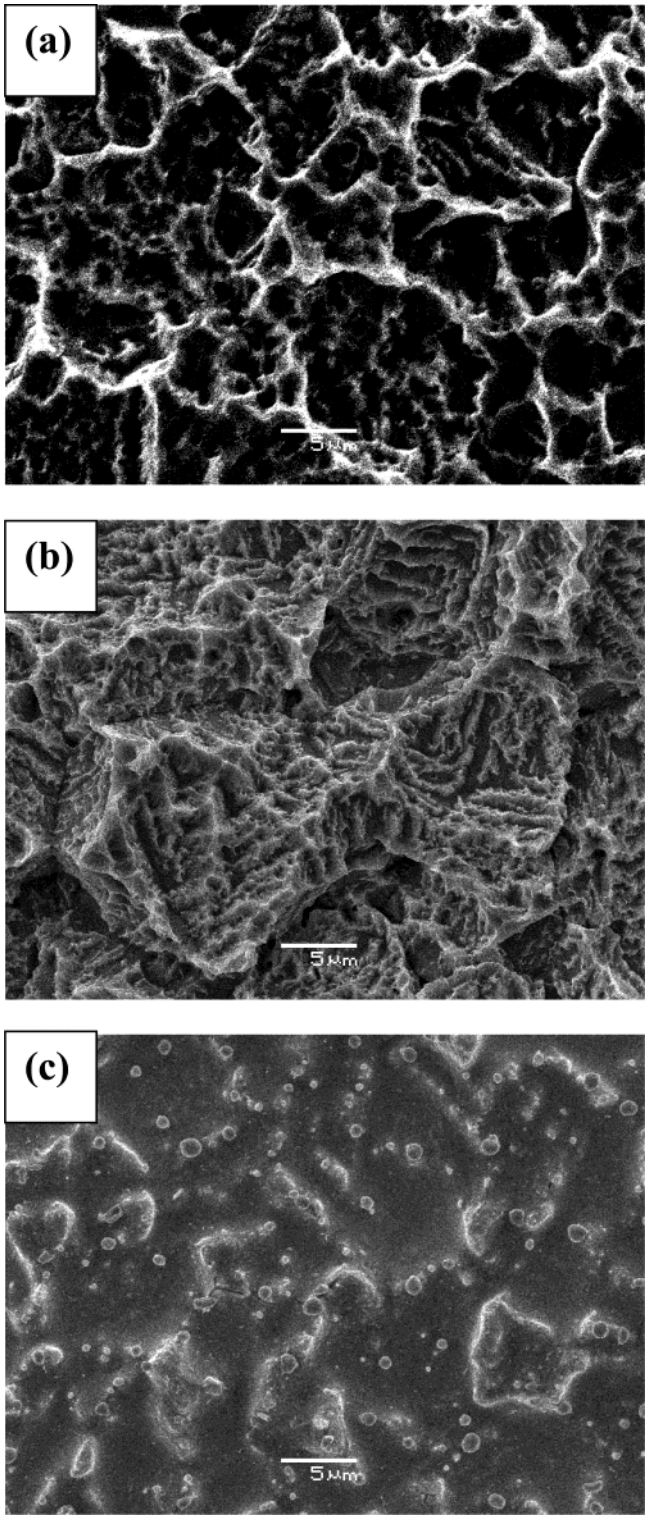

Figure 1. Scanning electron micrographs of various Ti surfaces: (a) after etching (Ti); (b) after etching and with a 2 min sputtering Au film (Ti/Au2); (c) after the oxide coating before electrochemical tests (Ti/Au2/SnO_2-Sb_2O_5). Magnification: 3000× (reproduced at 95% of original size).

The average load of the gold film was 0.13 mg/cm^2 for 1 min of sputtering and 0.26 mg/cm^2 for 2 min of sputtering. The

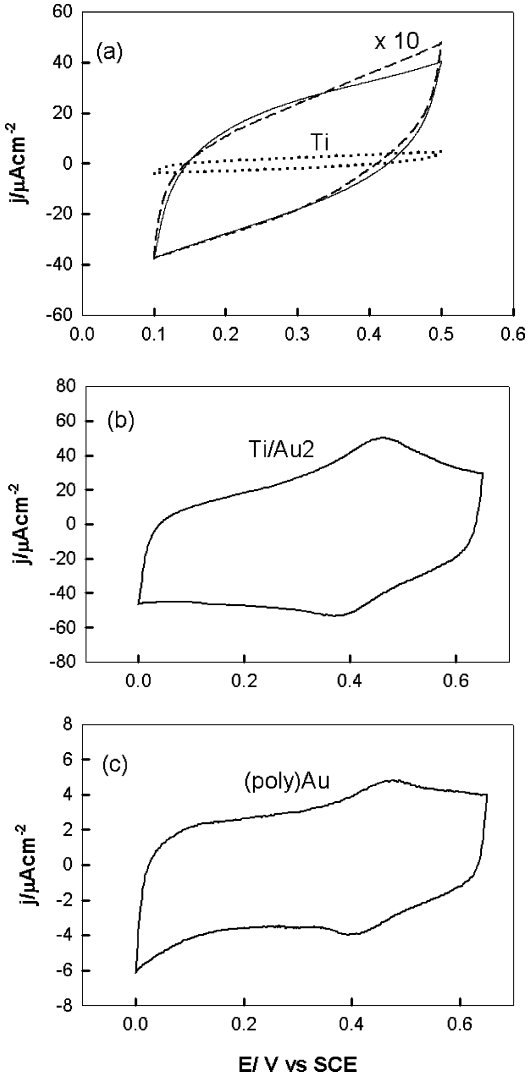

Figure 2. Cyclic voltammograms in 1.0 M H_2SO_4 of (a) polished Ti (dotted line and dashed line) and etched Ti (solid line), (b) etched Ti with a 2 min sputtering Au film (Ti/Au2), and (c) a polycrystalline Au electrode. Potential scan rate: 20 mV/s.

diameter of the Ti rod used in this study was 12 mm. However, one cannot use the geometric surface area of the etched Ti substrate to determine the thickness of the gold film as shown in both the SEM images in Figure 1a,b. The actual surface area of the etched Ti is much larger than its geometric surface area. To estimate the roughness of the etched Ti substrate, we applied CV to study the polished Ti substrate before and after being etched. Figure 2a shows two CV curves recorded in 1 M H_2SO_4 solution at a sweep rate of 20 mV/s for the polished Ti substrate (dotted line) and the polished and then etched Ti substrate (solid line). The surface of the polished Ti substrate was very smooth, like a mirror. As expected, the CV curve for the polished surface is much smaller than that for the etched Ti surface. Note that the CV curve of the polished Ti surface multiplied by 10 (the dashed curve) is almost identical to the CV curve of the etched Ti substrate. Therefore, the roughness factor ρ resulting from the etching process can be considered as 10. The voltammetric curves recorded in the double-layer region between the limits of hydrogen and oxygen evolution represent the total active area. The estimation of the roughness factor ρ is very approximate. As the gold film fabricated by the sputtering method is uniform, we may use the following equation to estimate the thickness ϕ of the thin gold film:

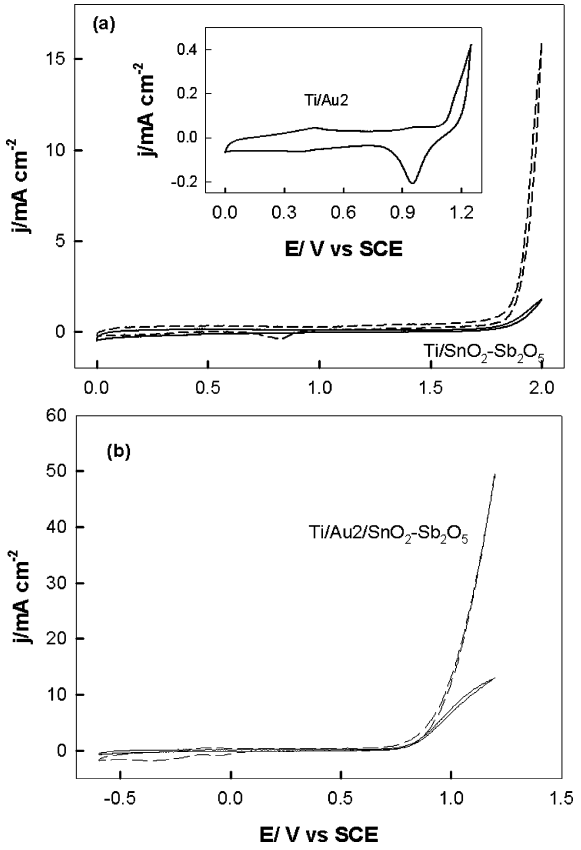

Figure 3. Cyclic voltammograms of (a) $Ti/Au1/SnO_2$-Sb_2O_5 (dashed line) and Ti/SnO_2-Sb_2O_5 (solid line) in 1.0 M H_2SO_4 and (b) $Ti/Au2/SnO_2$-Sb_2O_5 (dashed line) and Ti/SnO_2-Sb_2O_5 (solid line) in 1.0 M NaOH. Inset to (a): a CV curve of a gold film (Ti/Au2) in 1.0 M H_2SO_4. Potential scan rate: 20 mV/ s.

$$\phi = m/(\rho A \gamma)$$

where m is the weight of the gold film, A is the geometric surface area, and γ is the density of the gold. As a result, the thickness of the gold thin film was approximatly 6.8 nm for the 1 min sputtering (Ti/Au1) and around 13.6 nm for the 2 min sputtering (Ti/Au2). Cyclic voltammetry was further employed to characterize the electrochemical behavior of the nanoscale gold films.

Parts b and c of Figure 2 show two CV curves recorded in 1 M H_2SO_4 with a Ti/Au2 gold film and a polycrystalline Au electrode, respectively. It is interesting to notice that the shapes of these two CV curves are very similar: a broad positive-going band centered at 0.45 V during the positive-going sweep followed by a wide negative-going band at around 0.38 V during the negative-going sweep. This is due to the adsorption/desorption of sulfate ions.[28,29] These results show that the electrochemical behavior of the thin gold film Ti/Au2 is very similar to that of the polycrystalline Au electrode surface. Please note the *y* scale of the CV curve for Ti/Au2 is 10 times bigger than that for the polycrystalline Au electrode. The ratio of the integration of the first half-cycle of the CV curve (Figure 2b) for Ti/Au2 to the integration of the first half-cycle of the CV curve (Figure 2c) for the polycrystalline Au surface is 11, which is 10% bigger than the roughness factor ρ as expected.

3.2. Electrochemical Behavior of the Oxide Coatings. CV was used to characterize the SnO_2-Sb_2O_5 coatings. Figure 3a shows two CV curves of the oxide electrodes recorded at a sweep rate of 20 mV/s in 1.0 M H_2SO_4 with the nanoscale gold film thin layer (dashed line) and without a gold thin layer (solid line). The onset potential of oxygen evolution is 1.82 V/SCE

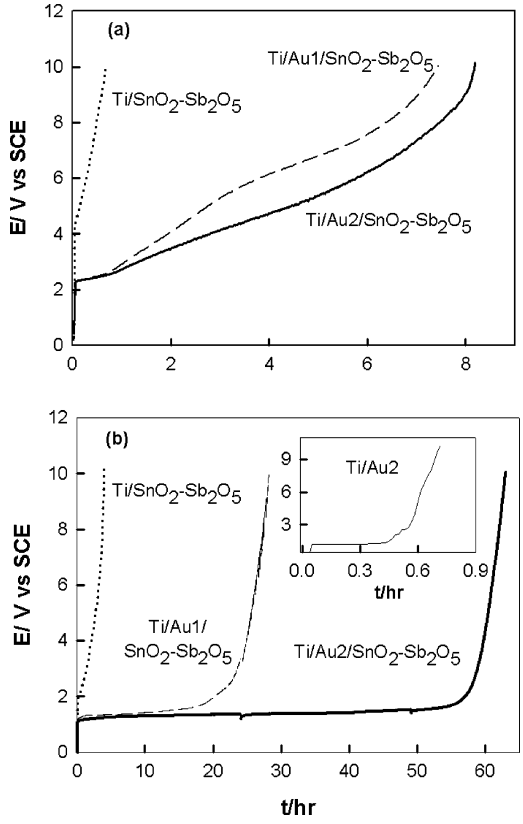

Figure 4. Accelerated service life tests on various tin and anitmony oxide based electrodes: (a) without Au film, Ti/SnO_2-Sb_2O_5 (dotted line), Ti/Au1/SnO_2-Sb_2O_5 (dashed line), and Ti/Au2/SnO_2-Sb_2O_5 (solid line) in 1.0 M H_2SO_4; (b) Ti/SnO_2-Sb_2O_5 (dotted line), Ti/Au1/SnO_2-Sb_2O_5 (dashed line), and Ti/Au2/SnO_2-Sb_2O_5 (solid line) in 1.0 M NaOH. The inset to (b) is of an accelerated test on a gold film Ti/Au2.

for the Ti/SnO_2-Sb_2O_5 electrode. In the CV curve of the Ti/Au1/SnO_2-Sb_2O_5 electrode, oxygen evolution starts at 1.78 V; further increasing the electrode potential increases the current exponentially. During the negative-going sweep, a broad band centered at 0.88 V is observed, which is due to the reduction of oxide formed at the higher potential. The inset to Figure 3a shows the CV curve of the Ti/Au2 electrode without an oxide coating recorded in 1.0 M H_2SO_4. The feature of this curve is consistent with those of the CV curves for the polycrystalline gold electrodes. The onset potential for oxygen evolution on Ti/Au2 is around 1.18 V, which is 640 mV lower than that on the Ti/SnO_2-Sb_2O_5 electrodes. To compare the effect of the pH of the electrolyte, Figure 3b shows two CV curves recorded in 1.0 M NaOH solution with the Ti/SnO_2-Sb_2O_5 (solid line) and Ti/Au1/SnO_2-Sb_2O_5 (dashed line) electrodes. The onset potential for oxygen evolution on the electrode with a gold thin film is slightly lower than that on the SnO_2-Sb_2O_5 coating without the gold film, and the current density for the oxygen evolution reaction on the Ti/Au1/SnO_2-Sb_2O_5 electrode is much higher. The effect of the presence of the nanoscale gold thin film on the service lifetime of the SnO_2-Sb_2O_5 coatings is shown in Figure 4.

Figure 4a shows three accelerated tests of the Ti/SnO_2-Sb_2O_5 (dotted line), Ti/Au1/SnO_2-Sb_2O_5 (dashed line), and Ti/Au2/SnO_2-Sb_2O_5 (solid line) electrodes in 1.0 M H_2SO_4 solution. The service lifetime of the SnO_2-Sb_2O_5 coatings without a gold film interlayer was very short, only 0.68 h. The presence of the 1 min sputtering gold thin film interlayer prolonged the service lifetime of the SnO_2-Sb_2O_5 coatings to 7.45 h. By further increasing the thickness of the gold film, the service lifetime of the Ti/Au2/SnO_2-Sb_2O_5 electrode reached 8.18 h, which is

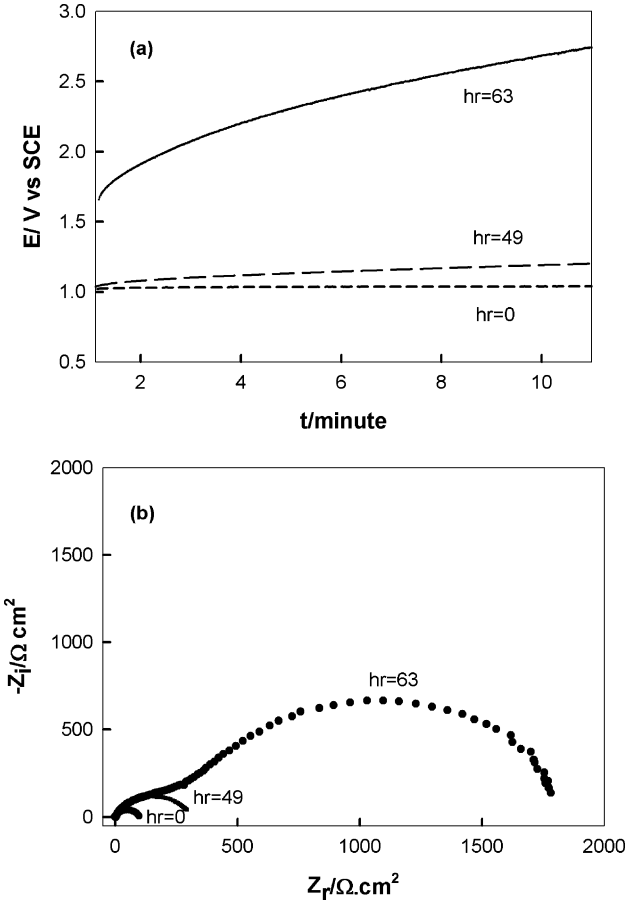

Figure 5. (a) Chronopotentiometric curves, 10 mA·cm^{-2}, and (b) EIS plots measured at the electrode potential −0.8 V vs SCE of a Ti/Au2/SnO_2-Sb_2O_5 electrode in 1.0 M NaOH before the lifetime test (short dashed line), after the 49 h lifetime test (dashed line), and after deactivation (solid line).

12 times longer than that of the SnO_2-Sb_2O_5 coating without the gold film interlayer. To investigate the effect of electrolytes, the accelerated test results of the Ti/SnO_2-Sb_2O_5 (dotted line), Ti/Au1/SnO_2-Sb_2O_5 (dashed line), and Ti/Au2/SnO_2-Sb_2O_5 (solid line) electrodes in 1.0 M NaOH solution are presented in Figure 4b. The service life of the SnO_2-Sb_2O_5 coatings was 4 h without a gold film interlayer, 26.7 h with a 1 min sputtering gold film interlayer and 64 h with a 2 min sputtering gold film interlayer. The service life of the oxide coating with a 13.6 nm gold film interlayer was 15.7 times longer than that without a gold film interlayer. The above results also show that the service life of the SnO_2-Sb_2O_5 coatings is much longer in the caustic solution than that in the acidic electrolyte. In both the basic and the acidic solutions, the presence of a thin gold film greatly increases the service life of the SnO_2-Sb_2O_5 coating. Now the question is whether the longer service life is due to the service lifetime of the gold thin films. To answer this question, we did further studies on the gold thin film. The accelerated test result of the Ti/Au2 electrode in 1.0 M NaOH is shown in the inset of Figure 4b. The service life of the 2 min sputtering gold film Ti/Au2 was 0.72 h. For the Ti/Au1 and Ti/Au2 electrodes, the accelerated stability tests showed that the service life in 1.0 M H_2SO_4 solution was 0.17 and 0.43 h, respectively. All these results indicate that the great increase in the service life of the SnO_2-Sb_2O_5 coatings with the nanoscale gold film interlayer is not due to the contribution of the service lifetime of the gold film. Later EIS study and SEM image investigation show that the presence of the gold film interlayer effectively prevents the growth of the TiO_2 resistive layer.

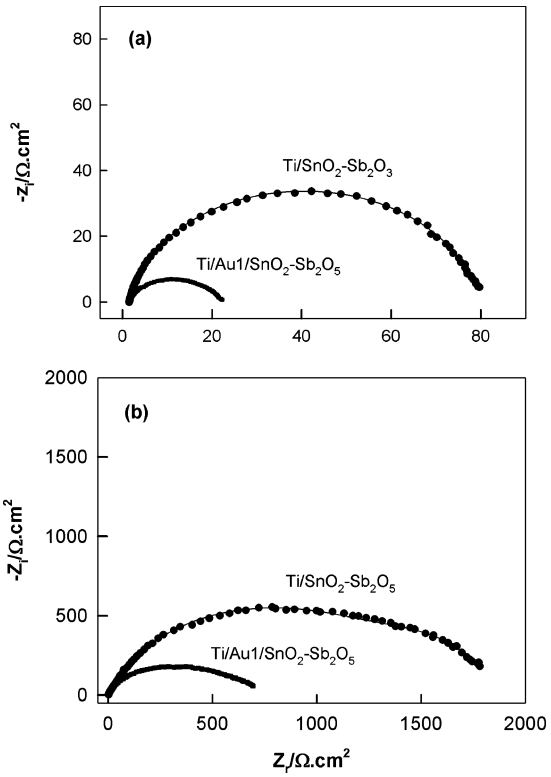

Figure 6. EIS complex plane plots in the 1 M acidic solution: (a) freshly prepared electrodes; (b) the electrode coating after deactivation. Experimental data: ● or △. Fitting curve: sold line. Electrode potential: 2.05 V vs SCE.

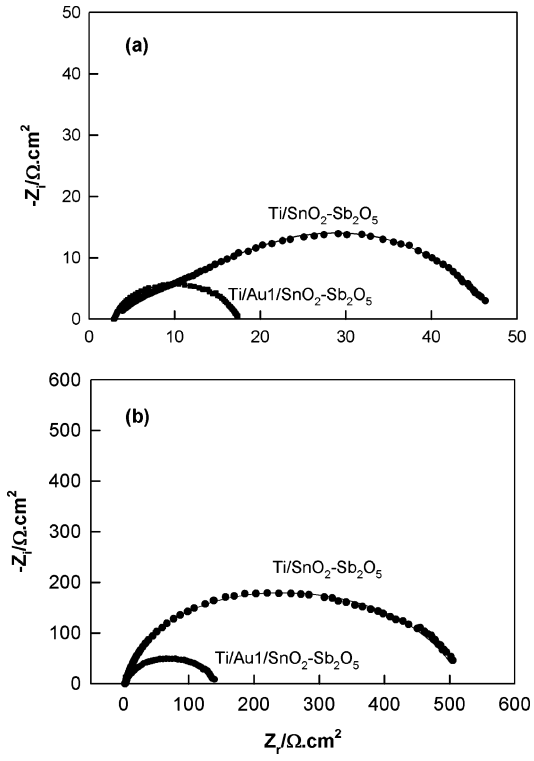

Figure 7. EIS complex plane plots in the 1 M NaOH solution: (a) freshly prepared electrodes; (b) the electrode coating after deactivation. Experimental data: ● or △. Fitting curve: sold line. Electrode potential: 1.05 V vs SCE.

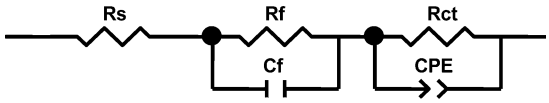

Figure 8. Equivalent circuit used in the simulation.

As shown in Figure 4b, at the end of the accelerated tests, the electrode potential increased rapidly from 1.6 to 10 V/SCE within 10 min. Thus, to understand the change of the oxide coatings before, during, and after the accelerated tests, a lower current was chosen for the chronopotentiometric studies. Figure 5a shows three chronopotentiometric curves of the Ti/Au2/SnO_2-Sb_2O_5 electrode at 10 mA·cm^{-2} in 1.0 M NaOH before the lifetime test (short dashed line), after the 49 h lifetime test (dashed line), and after the 63 h lifetime test (solid line). The anode potential only slightly increased after the 49 h lifetime test; however, there was a big increase in electrode potential between the dashed line and solid line, further indicating the deactivation of the electrode after the 63 h lifetime test. EIS is a powerful technique to study porous electrodes.[30−32] Figure 5b presents three EIS curves of Ti/Au2/SnO_2-Sb_2O_5 at the electrode potential 0.8 V in 1.0 M NaOH at hr = 0 (before the lifetime test), hr = 49 (after the 49 h lifetime test), and hr = 63 (after deactivation). The impedance spectra are very consistent with the chronopotentiometric results. The charge transfer resistance of the electrode slightly increased after the 49 h lifetime test; however, there was a big increase in the impedance after the electrode was deactivated.

3.3. Failure Mechanisms of the SnO_2-Sb_2O_5 Electrodes. To understand the failure mechanism and the effect of the Au thin film, we did further EIS and SEM studies. Figure 6 presents the complex plane plots for the freshly prepared (Figure 6a) and deactivated (Figure 6b) SnO_2-Sb_2O_5 coatings with and without the nanoscale gold film interlayer in a 1 M H_2SO_4 solution. For comparison, the electrochemical impedance behavior in a 1 M NaOH solution is also presented in Figure 7. The equivalent circuit shown in Figure 8 was used to fit the EIS data, and the fitting curves are shown in Figures 6 and 7 as solid lines together with the experimental data denoted as symbols. In this $R_s(R_fC_f)(R_{ct}\text{CPE})$ circuit, R_s represents the solution resistance, the parallel combination R_fC_f is associated with the properties of the films,[33,34] for instance, the nanoscale gold thin film, TiO_2 layer, and SnO_2-Sb_2O_5 coating, and the parallel combination of the charge-transfer resistance (R_{ct}) and the constant phase element (CPE) takes into account the oxygen evolution reaction (OER).[30,32] The combination $(R_{ct}C_{dl})L$ was applied to address the contribution of the OER to the impedance spectra for the IrO_2–TiO_2 films,[33] where C_{dl} is the capacitance of the double layer and L is an inductance. In addition, the parallel combination $R_{ct}C_{dl}$ was used to simulate the OER for the Ir-based ceramic oxides containing TiO_2 and SnO_2.[34] However, the replacement of R_{ct}CPE in the circuit with either $(R_{ct}C_{dl})L$ or $R_{ct}C_{dl}$ does not provide a good fit to our experimental data. The CPE is defined by CPE-T and CPE-P. If CPE-P equals 1, then the CPE is identical to a capacitor, C_{dl}. The parallel combination R_{ct}CPE leads to a depressed semicircle in the corresponding Nyquist impedance plot. In the present study, the fitting of the experimental data results in CPE-P $\approx$ 0.8, which is in excellent agreement with the EIS study of Ir + Ti + Pt ternary oxide electrodes conducted by Da Silva et al.[35] Thus, the CPE-T values obtained in this work are close to C_{dl} and represent the electrochemically active surface sites. The parameters R_f, C_f, R_c, and CPE-T and their associated errors (%) determined by the fitting of the experimental EIS data in the acidic and basic solutions are summarized in Tables 1 and 2, respectively. The error is within 8%, and the low error indicates the proposed model shown in Figure 8 can fit the experimental data effectively.

TABLE 1: Impedance Components for OER on Tin and Antimony Oxide Electrodes Determined by Fitting the Experimental Data Measured in 1.0 M H_2SO_4 at 2.05 V/SCE Using the Equivalent Circuit Shown in Figure 8

	R_f (Ω cm^2)		C_f (mF cm^{-2})		R_{ct} (Ω cm^2)		CPE-T (mF cm^{-2})	
electrode	value	error (%)	value	error (%)	value	error (%)	value	error (%)
Ti/SnO_2-Sb_2O_5 fresh	37.9	1.7	1.38	1.9	41.6	0.4	3.17	0.9
Ti/ SnO_2-Sb_2O_5 deactivated	410.0	4.2	0.93	5.3	1411.0	1.4	0.051	0.3
Ti/Au1/SnO_2-Sb_2O_5 fresh	3.7	3.9	1.08	4.3	17.1	0.9	2.16	1.2
Ti/Au1/SnO_2-Sb_2O_5 deactivated	212.5	3.9	0.77	4.7	450.5	1.6	0.068	0.5

TABLE 2: Impedance Components for OER on Tin and Antimony Oxide Electrodes Determined by Fitting the Experimental Data Measured in 1.0 M NaOH at 1.05 V/SCE Using the Equivalent Circuit Shown in Figure 8

	R_f (Ω cm^2)		C_f (mF cm^{-2})		R_{ct} (Ω cm^2)		CPE-T (mF cm^{-2})	
electrode	value	error (%)	value	error (%)	value	error (%)	value	error (%)
Ti/SnO_2-Sb_2O_5 fresh	15.8	2.0	0.35	2.1	31.3	1.3	1.38	2.7
Ti/SnO_2-Sb_2O_5 deactivated	125.9	4.2	0.30	4.1	391.0	2.5	0.070	3.6
Ti/Au1/SnO_2-Sb_2O_5 fresh	0.73	2.5	0.17	2.7	14.2	1.8	0.58	3.4
Ti/Au1/SnO_2-Sb_2O_5 deactivated	26.6	7.4	0.12	6.1	114.0	3.2	0.24	5.1

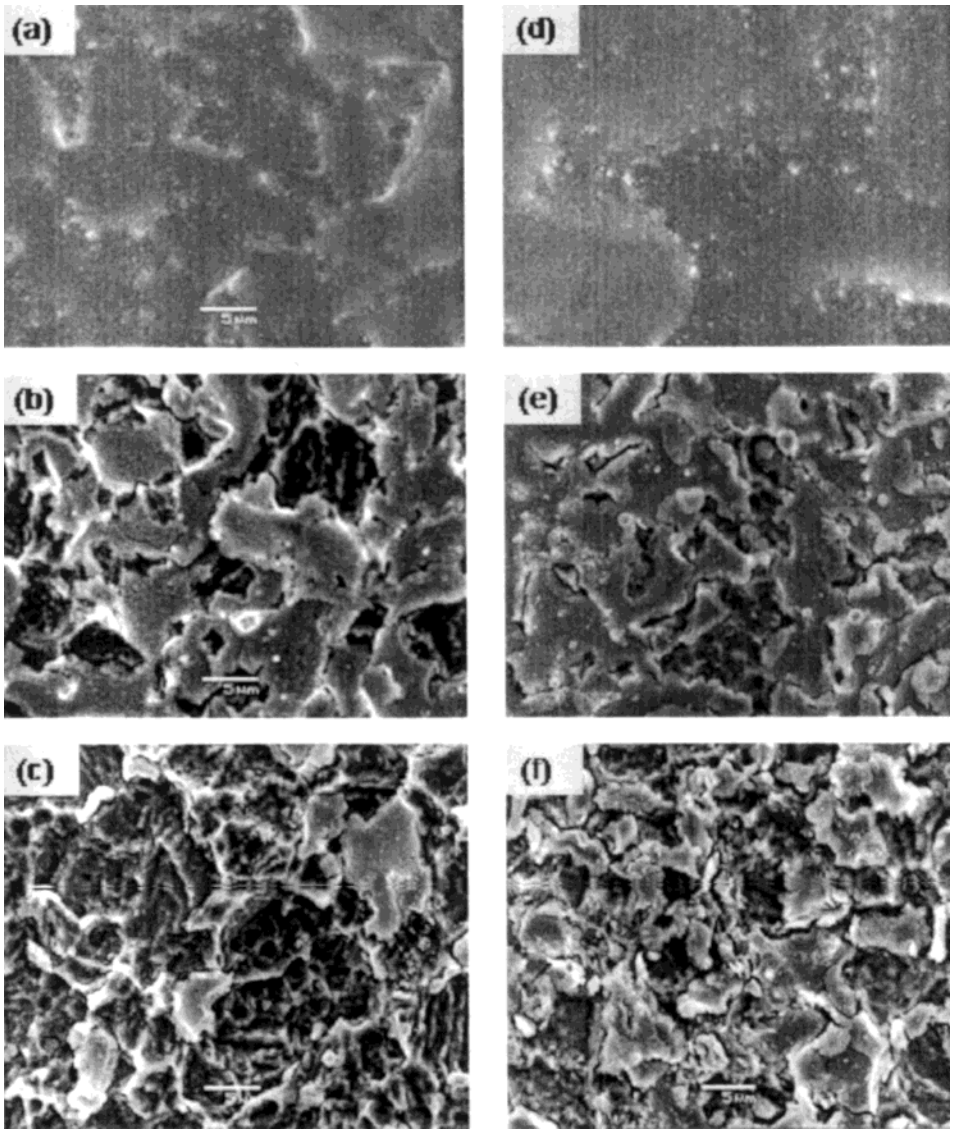

Figure 9. SEM images of various failed tin and antimony oxide based electrodes after the accelerated tests in the 1 M H_2SO_4 solution (a−c) or in the 1 M NaOH solution (d−f): samples a and d, Ti/SnO_2-Sb_2O_5; samples b and e, Ti/Au1/SnO_2-Sb_2O_5; samples c and f, Ti/Au2/ SnO_2-Sb_2O_5. Magnification: 3000×.

The values of these parameters depend on the applied electrode potential.[33] In this study, there were two categories of electrode samples: deactivated in the acid and failed in the basic electrolyte. A potential of 2.05 V in 1.0 M H_2SO_4 was chosen for the EIS study of the samples before and after the accelerated tests in the acid; a potential of 1.05 V in 1.0 M NaOH was chosen for the EIS study of the samples before and after the accelerated tests in the caustic solution. As shown in Figure 3, these two potentials are located in the oxygen evolution reaction range. Four major features can be seen from Tables 1

and 2: (1) The values of all these parameters strongly depend on the electrolytes. For all of the freshly prepared electrodes, with or without the gold thin layer, all four parameters have a lower value in the caustic solution than in the acidic medium. This may be due to the applied electrode potential and the nature of the electrolytes. High pH always favors the oxygen evolution reaction. As observed in Figure 3, the oxygen evolution on the electrodes in 1 M NaOH at the electrode potential $E = 1.1$ V/SCE is even stronger than that in 1 M H_2SO_4 at $E = 2.05$ V/SCE. (2) The R_f of all the freshly prepared electrodes with the gold thin film interlayer is much smaller than that of the electrodes without the gold thin layer. This is in agreement with the incorporation of a gold layer between the Ti substrate and the PbO_2 decreasing the resistance of the electrode as observed by Comninellis and Plattner.[36] It is known that the thermal procedure applied for the oxide coating fabrication always results in the growth of a thin TiO_2 film between the substrate (Ti) and the oxide coating. The much lower R_f of the freshly prepared electrodes with the nanoscale gold layer indicates that the presence of the gold thin film prevents the growth of the insulating TiO_2 layer effectively during the thermal fabrication procedure. (3) The deactivated electrodes have much larger R_f and R_{ct} compared with the corresponding freshly prepared electrodes; in contrast, the C_f and CPE-T became smaller after the deactivation. (4) Finally, the samples that deactivated in the acidic solution have much larger R_f and R_{ct} than those that failed in the caustic electrolyte. To understand these changes, we further investigated the deactivated electrodes using SEM. Figure 9 presents six SEM micrographs of the failed oxide electrodes after the lifetime tests performed either in the acidic solution (a−c) or in the basic electrolyte solution (d−f). There was no gold thin film on samples a and d, and the thickness of the gold film interlayer was 6.8 nm for samples b and e and 13.6 nm for samples c and f. It is interesting to notice that the amount of oxide coating left strongly depends on the screening electrolytes and the presence of the gold thin film, although the lifetime tests of all six samples were stopped at the same anode potential of 10 V vs SCE. As seen in Figure 4, the service life changed in the following order:

(a) Ti/SnO_2-Sb_2O_5 ≪ (b) Ti/Au1/SnO_2-Sb_2O_5 < (c) Ti/Au2/SnO_2-Sb_2O_5 (in the acid)

(d) Ti/SnO_2-Sb_2O_5 ≪ (e) Ti/Au1/SnO_2-Sb_2O_5 < (f) Ti/Au2/SnO_2-Sb_2O_5 (in the caustic solution)

In contrast, as shown in Figure 9, the SEM micrographs for the failed samples a and d are very similar to those presented in Figure 1c for the unused SnO_2-Sb_2O_5 electrode, which indicates that there is still a fair amount of SnO_2-Sb_2O_5 coating remaining on samples a and d. The SEM micrographs show much less coating remaining on samples b and e. In addition, the R_f and R_{ct} of samples a and d are much larger than those of samples b and e. All these results indicate that (1) the failure of samples a & d is mainly due to the formation of an insulating TiO_2 layer between the Ti substrate and the catalyst coating during the lifetime tests and (2) the presence of the gold thin film effectively prevents the growth of a TiO_2 layer. Very little coating left on the electrodes with a 2 min sputtering of gold film shows that the failure of samples c and f is caused mainly by coating consumption.

4. Conclusions

The nanoscale gold thin film and its influence on the Ti/SnO_2-Sb_2O_5 coating have been investigated by the SEM image technique and electrochemical methods such as cyclic voltammetry, electrochemical impedance spectroscopy, and the chronopotentiometric technique. The cyclic voltammetry study shows that the etching process increases the surface area of the Ti substrate 10-fold. The gold thin film was fabricated using a sputtering method, and the thickness of the gold film was approximately 6.8 nm for 1 min of sputtering and around 13.6 nm for 2 min of sputtering, estimated by the electrochemical methods. The nanoscale gold thin film has electrochemical behavior very similar to that of a polycrystalline Au electrode. We have demonstrated that the presence of a nanoscale Au thin film on a Ti substrate can effectively prevent the formation of a TiO_2 insulating layer between the substrate and oxide coating, resulting either from the thermal procedure during the oxide electrodes' fabrication or from the electrochemical process during lifetime tests. Consequently, the presence of a 13.6 nm gold thin film prolongs the service lifetime of the SnO_2-Sb_2O_5 electrodes 12-fold in the acidic solution and over 15-fold in the basic electrolyte. The EIS and SEM studies have shown that (1) the deactivation of the SnO_2-Sb_2O_5 electrodes without a gold thin film is mainly due to the formation of the insulating TiO_2 layer between the Ti substrate and the catalyst during the lifetime tests and (2) the failure of the electrodes with a gold thin layer is mainly caused by coating consumption.

Acknowledgment. This work was supported by a grant from the Natural Sciences and Engineering Research Council of Canada (NSERC). We express our gratitude to Mr. Al Mackenzie for his assistance in imaging some samples with the SEM in the Lakehead University Instrumentation Laboratory.

References and Notes

(1) Beer, H. B. Br. Patent 1 147 442, 1965.
(2) Trasatti, S. *Electrochim. Acta* **2000**, *45*, 2377.
(3) Trasatti, S. In *The Electrochemistry of Novel Materials*; Lipkowski, J.; Ross, P. N., Eds.; VCH Publishers: New York, 1994.
(4) Moreland, P. J.; Howell, K. M. In *Cathodic Protection Theory and Practice*; Ashworth, V., Googan, C., Eds.; Ellis Horwood Ltd.: Chichester, U.K., 1993.
(5) Xu, L. K.; Scantlebury, J. D. *J. Electrochem. Soc.* **2003**, *150* (6), B254.
(6) Bock, C.; MacDougall, B. *J. Electroanal. Chem.* **2000**, *491*, 48.
(7) Gattrell, M.; MacDougall, B.; Henuset, Y. M.; Fournier, J. *J. Appl. Electrochem.* **2002**, *32*, 1303.
(8) Chen, G. H.; Chen, X. M.; Yue, P. L. *J. Phys. Chem. B* **2002**, *106*, 4364.
(9) Tsiplakides, D.; Nicole, J.; Comninellis, Ch. *J. Electrochem. Soc.* **1997**, *144*, L312.
(10) Trasatti, S. In *Modern Chlor-Alkali Technology*; Curry, R. W., Ed.; Royal Society of Chemistry: Cambridge, 1995; Vol. 6, p 110.
(11) Pilla, A. S.; Cobo, E. O.; Duarte, M. M. E.; Salinas, D. R. *J. Appl. Electrochem.* **1997**, *27*, 1283.
(12) Ferro, S.; De Battisti, A. *J. Phys. Chem. B* **2002**, *106*, 2249.
(13) Correa-Lozano, B.; Comninellis, Ch.; De Battisti, A. *J. Appl. Electrochem.* **1997**, *27*, 970.
(14) Vercesi, G. P.; Rolewicz, J.; Comninellis, Ch.; Hinden, J. *Thermochim. Acta* **1991**, *176*, 31.
(15) Comninellis, Ch.; Vercesi, G. P. *J. Appl. Electrochem.* **1991**, *21*, 335.
(16) De Pauli, C. P.; Trasatti, S. *J. Electroanal. Chem.* **2002**, *538*, 145.
(17) Martelli, G. N.; Ornelas, R.; Faita, G. *Electrochim. Acta* **1994**, *39*, 1551.
(18) Pilla, A. S.; Cobo, E. O.; Duarte, M. M. E.; Salinas, D. R. *J. Appl. Electrochem.* **1997**, *27*, 1283.
(19) Lassali, T. A. F.; Boodts, J. F. C.; Bulhoes, L. O. S. *J. Appl. Electrochem.* **2000**, *30*, 625.
(20) Tilak, B. V.; Chen, C. P.; Birss, V. I.; Wang, J. *Can. J. Chem.* **1997**, *75*, 1773.
(21) Rodgers, J. D.; Jedral, W.; Bunce, N. J. *Environ. Sci. Technol.* **1999**, *33*, 1453.

(22) Park, S.; Tong, Y.; Wieckowski, A.; Weaver, M. J. *Langmuir* **2002**, *18*, 3233.
(23) Tong, Y. Y.; Kim, H. S.; Babu, P. K.; Waszczuk, P.; Wieckowski, A.; E. Oldfield, E. *J. Am. Chem. Soc.* **2002**, *124*, 468.
(24) Haruta, M. *CATTECH* **2002**, *6*, 102.
(25) Luo, J., Jones, V. W.; Maye, M. M.; Han, L.; Kariuki, N. N.; C. J. Zhong, C. J. *J. Am. Chem. Soc*. **2002**, *124*, 13988.
(26) Maye, M. M.; Luo, J.; Lin, Y.; Engelhard, M. H.; Hepel, M.; Zhong, C. J. *Langmuir* **2003**, 125.
(27) Chen, A.; Lipkowski, J. *J. Phys. Chem. B* **1999**, *103*, 682.
(28) Shi, Z.; Lipkowski, J.; Gamboa, M.; Zelenay, P.; Wieckowski, A. J. *Electroanal. Chem.* **1994**, *366*, 317.
(29) Shi, Z.; Lipkowski, J.; Mirwald, S.; Pettinger, P. *J. Electroanal. Chem.* **1995**, *396*, 115.
(30) Retter, U. In *Electroanalytical Methods*: *Guide to Experiments and Applications*; Scholz, F., Ed.; Springer-Verlag: Berlin, Heidelberg, New York, 2002.
(31) Hitz, C.; Lasia, A. *J. Electroanal. Chem*. **2001**, *500*, 213.
(32) Lasia, A. In *Modern Aspects of Electrochemistry*; Conway, B. E., White, R. E., Eds.; 2002; Vol. 35.
(33) Da Silva, L. A.; Alves, V. A.; Da Silva, M. A. P.; Trasatti, S.; Boodts, J. F. C. *Electrochim. Acta* **1997**, *42*, 271.
(34) Lassali, T. A. F.; Boodts, J. F. C.; Bulhoes, L. O. S. *J. Appl. Electrochem*. **2000**, *30*, 625.
(35) Da Silva, L. A.; Alves, V. A.; Da Silva, M. A. P.; Trasatti, S.; Boodts, J. F. C. *Electrochim. Acta* **1996**, *41*, 1279.
(36) Comninellis, Ch.; Plattner, E. *J. Appl. Electrochem.* **1982**, *12*, 399.